The Structure and Deformation Behavior of Zinc-Rich Coatings on Steel Sheet

S.R. Shah, J.A. Dilewijns, and R.D. Jones

The deformation behavior of commercially produced hot-dipped zinc and zinc-alloy coatings on steel under simple uniaxial tension has been studied. The strong basal plane texture of the hot-dipped galvanized coatings was found to be unfavorable for plastic flow and accounted for the extensive cracking observed during deformation. The eutectic structure in Galfan coatings was found to be beneficial in suppressing the formation of microcracks at low strain levels, although when grain boundary dents were present, cracks formed easily at these locations. Microcracks were observed in Galvalume coatings at all levels of strain. A technique to measure the coating plasticity has been developed to quantify the level of cracking in coatings at varying degrees of deformation.

Keywords
deformation, Galfan, Galvalume, galvanized coatings

1. Introduction

THE DEFORMATION processes of zinc and zinc-alloy coatings on steel sheet are complex because of the different mechanical properties of the steel substrate, the coatings, and any intermetallic layers which are present. Zinc and zinc-alloy coatings must have the ability to be formed without extensive fracturing or peeling off the steel substrate or producing any unacceptable topographical changes in the outer coating layer, such as excessive roughening. Coating ductility depends on factors such as the grain size, crystallographic orientation, temperature, coating thickness, and thickness and phase composition of the intermetallic layer. This investigation has examined the deformation behavior of three types of commercially important hot-dip coatings: galvanized, Galfan,* and Galvalume.**

The deformation behavior in hexagonal close-packed metals such as zinc is well documented (Ref 1-5). Slip occurs on the basal (0001) plane and in the $\langle 11\bar{2}0 \rangle$ directions. Plastic deformation is also accomplished by pyramidal slip and/or deformation twinning. Twinning becomes more important under conditions where pyramidal slip, which is thermally activated, is not favorable or where the basal plane is unfavorably oriented for slip. One contributing effect of twinning to general plastic flow is that unfavorably oriented grains for slip are reoriented into a more favorable position upon twinning. Cleavage in zinc crystals occurs mainly on primary basal planes or on secondary cleavage planes, which are basal planes in twins formed prior to fracture.

*Galfan is a registered tradename owned by the International Lead Zinc Research Organization (ILZRO).
**Galvalume is a registered trademark of Bethlehem Steel Corporation.

S.R. Shah, Bartlett Engineering, Metairie, LA 70002, USA, **J.A. Dilewijns,** University of Ghent, Ghent, Belgium, and **R.D. Jones,** North East Wales Institute, Wales, U.K.

2. Experimental Procedure

Details of the materials examined are given in Table 1. All were supplied by producers in Europe and North America.

Optical and scanning electron microscopy (SEM) were used to characterize the coating surface. Polarized light was found to be particularly helpful in resolving structures. All coated sheet samples were deformed in tension on a microscope-mounted straining stage at a strain rate of about 8×10^{-5}/s. Each specimen was strained to 5% engineering strain in small (~1%) increments. Further straining was then performed in 5% increments. The topography of the coating was examined after each deformation increment using the optical microscope, and where necessary, the SEM. The optical microscope used in this investigation was the Reichert-Jung Polyvar-Met, while the SEM used was a JEOL JSM-CF, fitted with a LINK energy dispersive analysis system.

X-ray diffraction was used to determine the texture of the coatings. The experiments were performed using a Philips PW1729 x-ray generator with a PW1710 diffractometer system. Cu-K_α radiation was used at 35 kV and 40 mA. Data

Table 1 Description of samples used

Identification	Coating type	Supplier's designation	Sheet gage, mm	Spangle size, mm	Coating weight, g/m²	Coating thickness, μm	
						Side I	Side II
GA	Galvanized	A	0.72	5.50	365	25	25
GF8	Galfan	B	0.70	0.33	135	8	8
GF15	Galfan	B	0.70	0.21	210	15	15
GF20	Galfan	C	0.70	0.05	250	20	20
GF23	Galfan	B	0.75	0.15	300	23	23
GL	Galvalume	A	0.50	2.60	240	20	20

collection and analysis were computer controlled and carried out by a Philips W1877 PC-APD analytical software package. The densities of the various (hkl) planes were determined by measuring the area under the peaks on the diffractograms. The calculated values averaged from several samples were then compared with those obtained from a random powder sample to give a comparative value. Details are given elsewhere (Ref 6, 7).

In a procedure used to measure the coating plasticity, micrographs were taken of all the samples after deformation to various degrees. The microplasticity was determined in samples in uncracked regions by measuring the distance between prominent microstructural features at different levels of strain. This method is helpful in particular for Galfan, which showed extensive plastic deformation.

3. Results and Discussion

3.1 *Structure and Texture of As-Received Samples*

The typical surface topography of a hot-dip galvanized coating consists of flat, single-ridged, and double-ridged grains

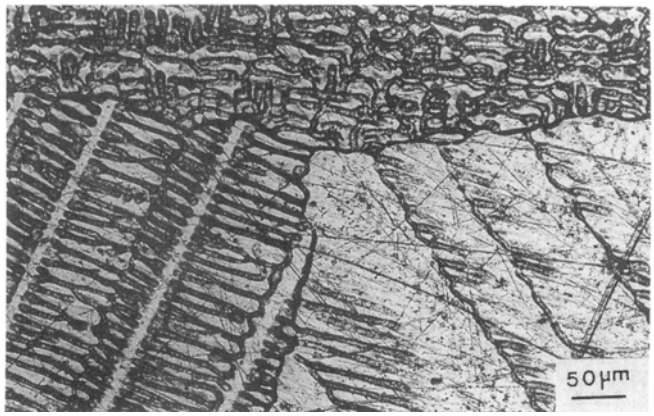

(a)

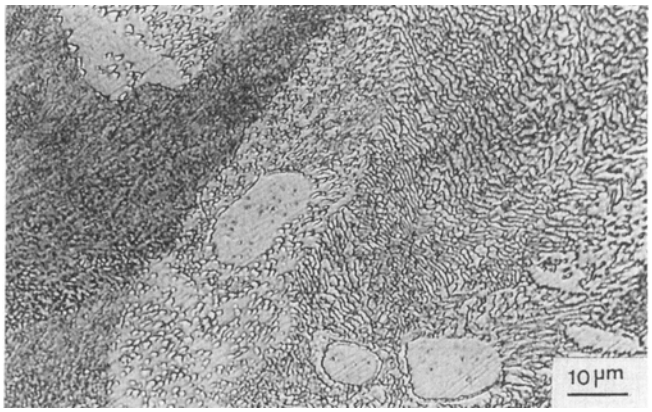

(b)

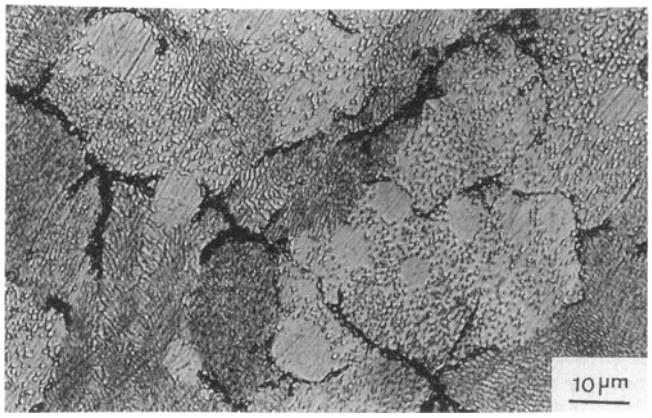

(c)

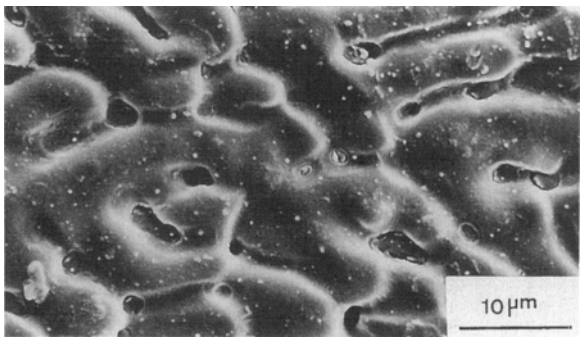

(d)

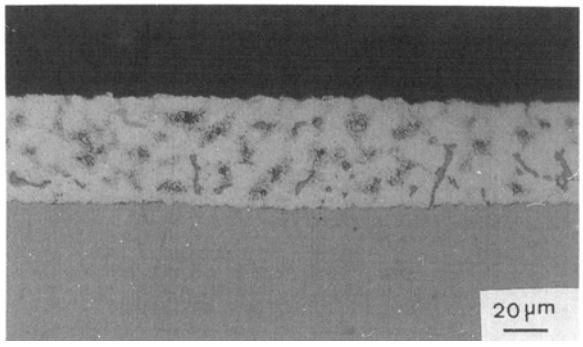

(e)

Fig. 1 (a) Galvanized—surface topography. (b) Galfan GF8—surface microstructure. (c) Galfan GF20—surface microstructure. (d) Galvalume—surface topography. (e) Galvalume—transverse microstructure

(Fig. 1a). The spangle topography has been described previously (Ref 8, 9). Many galvanized coatings show large numbers of grains with basal planes parallel to the surface. These grains tend to show a flat topography. The basal preferred orientation also becomes more pronounced in minimized coatings. Figure 2(a) shows a strong basal preferred orientation in the galvanized sample examined. However, it should be noted that the dull and frosty regions that have a dimpled and ridged structure (Ref 10) are evidence that the level of non-basal orientation is significant.

The microstructure of zinc-aluminum near-eutectic Galfan consists of two phases: zinc-rich particles surrounded by a typical eutectic phase consisting of white zinc (thick) and dark aluminum (thin) lamellae (Fig. 1b). The phase composition is affected by the cooling rate after galvanizing and by the bath composition (i.e., the aluminum content). A Galfan coating with a hypoeutectic composition (4.5% Al) produced at a high cooling rate will give a more uniform and homogeneous eutectic structure (Ref 11-13). The fineness of the microstructure is dependent on the cooling rate and becomes completely eutectic when fast cooled. Figure 1(c) shows one of the problems of the Galfan coating, the occurrence of shrinkage valleys (or dents) at grain boundaries, which represent localized regions of thin coating. These tend to promote grain boundary separation when deformed.

Table 2 shows the orientation data of the basal, pyramidal, and prismatic planes obtained for different regular and minimized spangle Galfan coatings. These intensities were obtained from planes parallel to the sheet surface. For each sample, the relative peak intensities were normalized to the maximum peak (Ref 14). The texture of a Galfan coating is seen to depend mainly on two factors: the coating weight and the spangle size, and therefore indirectly the cooling rate of the liquid. There is no previous work available on the first aspect of texture dependency, but there are various reports available on the second (Ref 15, 16). In the present study all Galfan coatings showed a preferred basal orientation. This is consistent with the report (Ref 14) that a strong basal plane texture develops in the hot-dipped coatings like Galfan when intermetallic compounds are very thin or not formed. It was also noted that the basal texture increased with thickness in coatings from the same source (GF8, GF15, GF23). Sample GF20, from a different source, is reported to have been given a minimizing treatment. This sample also shows an increased number of zinc-rich primaries (Fig. 1c) than other Galfan coatings. It shows a stronger basal texture than the thicker GF23 coating.

Table 2 Normalized intensities of peaks obtained on Galfan coatings

Plane	Ir(a)	Intensity, %			
		GF8	GF15	GF20	GF23
Basal					
(0002)	53	100	100	100	100
Pyramid					
$(10\bar{1}1)$	100	18	14	7	13
$(10\bar{1}2)$	28	3	2	2	2
$(10\bar{1}3)$	25	4	3	2	3
$(11\bar{2}2)$	23	2	2	1	1
Prism					
$(10\bar{1}0)$	40	4	7	7	6
$(11\bar{2}0)$	21	2	2	1	1

(a) Normalized intensities of peaks for randomly oriented zinc polycrystals

The Galvalume coating consists of two well-differentiated regions: a dendritic α-aluminum solid solution, which solidifies first, and a zinc-rich phase mixture, which fills in the interdendritic spaces of the α-phase. The zinc-rich phase mixture consists mainly of a zinc-aluminum eutectic, which forms as a result of nonequilibrium solidification (coring). A completely solidified coating will contain about 80% α dendrites and 20% zinc-rich phase mixture (Ref 17). These phases can be seen in Fig. 1(d) and (e). Shrinkage cavities can also be seen within the zinc-rich eutectic structure. Silicon is added to the alloy to limit intermetallic layer growth and thus improve coating adhesion. Silicon-rich particles can be seen in the transverse section (Fig. 1e).

The x-ray diffractogram of the Galvalume coating (Fig. 2b) shows a strong aluminum (111) texture. There is also a significant zinc $(10\bar{1}1)$ presence.

3.2 *Deformation Behavior of Zinc and Zinc-Alloy Coatings*

3.2.1 Hot-Dip Galvanized

Figure 3 shows typical examples of surface topographies (a, b, e, f) and transverse sections (c, d) of deformed samples. The

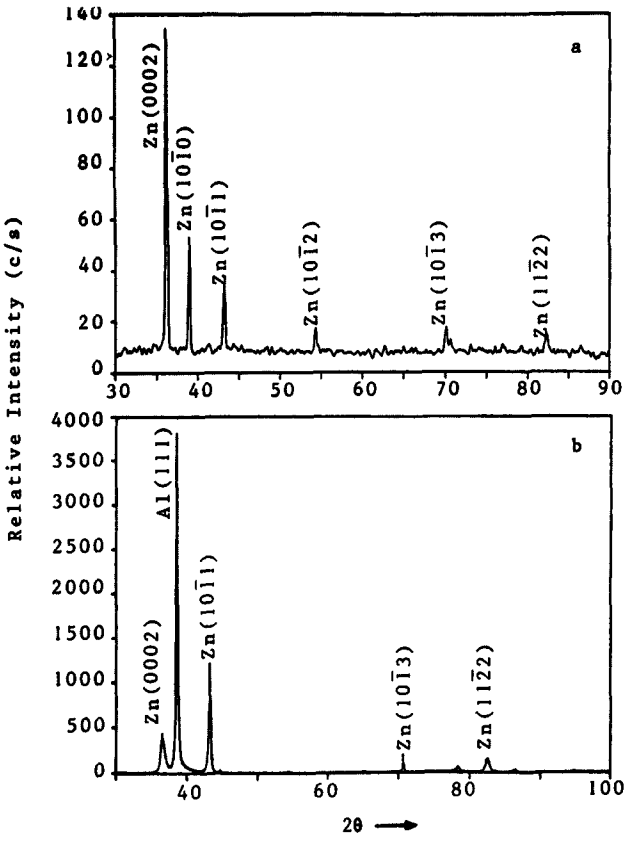

Fig. 2 Portions of x-ray diffractograms obtained on (a) galvanized and (b) Galvalume coating

deformation of regular spangle galvanized coating occurred primarily by twinning at low levels (<5%) of tensile strain. Twins are seen in Fig. 3(a) and (b) in both flat and ridged regions, and they are also evident in the transverse sections (Fig. 3c, d). Grain boundary separation increased with strain and probably initiates at the smallest strains.

At higher strains, intragranular cracks associated with basal plane (0001) cleavage predominate in basally oriented grains. It has been suggested (Ref 9) that intragranular cracking could occur by cleavage on matrix basal planes, provided that they were inclined at more than 12° to the plane of the surface or by secondary basal cleavage in twins in basally or nearly basally

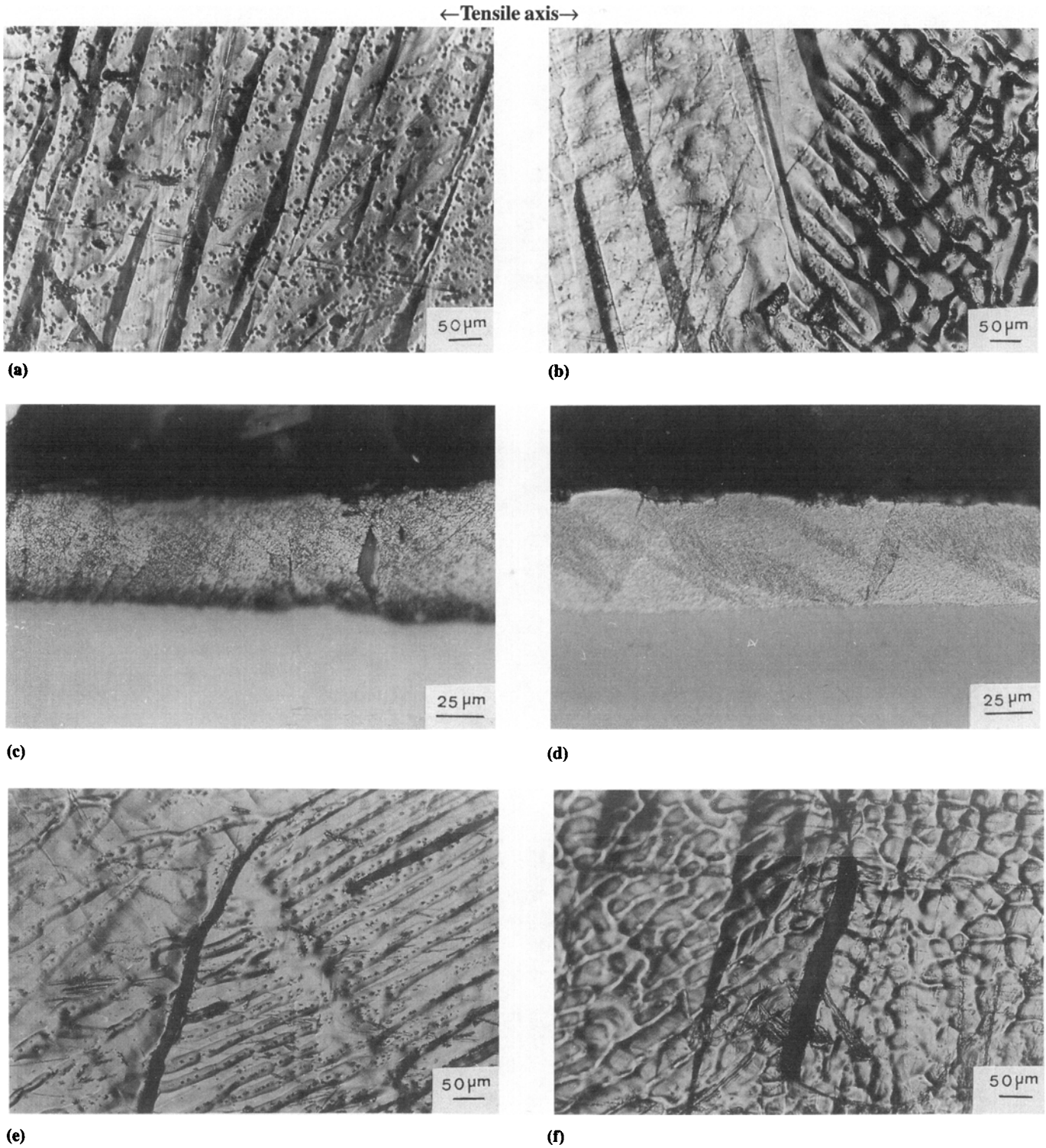

Fig. 3 Deformation of galvanized coating; twin formation at 4% strain in (a) shiny and (b) shiny and frosty spangle. (c) and (d) Transverse sections showing cracks within zinc layer at 10% and twin at 20% strain, respectively. (e) and (f) Cracks at grain boundary and along the ridges and intragranular cracking at 10% and 20% strain, respectively

oriented grains. This type of cracking has been reported (Ref 5). Evidence of cracking at twin bands at higher strains can also be seen in Fig. 3(c) and (d). In non-basally oriented grains, cracking was found along the ridges at higher strains (Fig. 3e), while large intragranular cracks are also evident in Fig. 3(f) at almost 90° to the tensile axis.

3.2.2 Galfan

The important factors that affect the behavior of a Galfan coating during a forming operation are the microstructure, texture, and thickness of the coating. The microstructure of the four coatings studied consisted of zinc-rich primaries dispersed within a eutectic matrix. All coatings exhibited a strong basal texture.

Two types of behavior were observed. In coatings GF8, GF15, and GF23, the first stage of deformation was plastic flow accommodated by slip and twinning. Figure 4 shows the deformation behavior over the strain range between 5 and 30%. Virtually no cracking was observed at low levels of strain. Evidence of plastic deformation is the extensive surface rumpling (Fig. 5) and the fine slip lines observed under polarized light (Fig. 5b). At higher strains, intragranular cracks were evident (Fig. 4), but there was also evidence of plastic flow without cracking. The formation of twins in the zinc primaries within the eutectic matrix at 60 to 80° to the tensile axis was observed at 5% strains (transverse section in Fig. 6a). Figure 6(b) shows a crack at the interface of the zinc primary and the matrix at 25% strain. In the thickest coating, GF23 (which displays a higher basal orientation and a smaller grain size), a greater susceptibility to cracking was found. The deformation mechanisms were again slip and twinning, but cracking was predominantly at grain and cell boundaries.

Coating GF20 behaved differently than coatings GF8, GF15, and GF23. Surface rumpling indicated that plastic deformation was again taking place, but the most important factor was the large number of grain boundary dents (Fig. 1c). These provided preferential sites for crack nucleation, as is shown by extensive grain boundary cracking at higher strains (Fig. 4). Intragranular cracks were also observed, but at lower strain levels than in coatings GF8, GF15, and GF23. This is a result of secondary basal cleavage in the higher number of zinc-rich primaries in this coating. The formation of twins prior to cracking was also observed, together with some intergranular cracks at a lower level of strain (Fig. 7a).

The size of twins in Galfan appears to be related to the initial grain size. In the larger grain size coatings (e.g., GF8 and GF15), coarser twins were observed (Fig. 7b). The larger grain size coatings also contained less basally oriented grains, as shown in Table 2. These results are in agreement with previous findings (Ref 7) that in galvanized coatings, the localization of twinning strain is less extensively developed with a larger grain size than with a small grain size under the same conditions. In

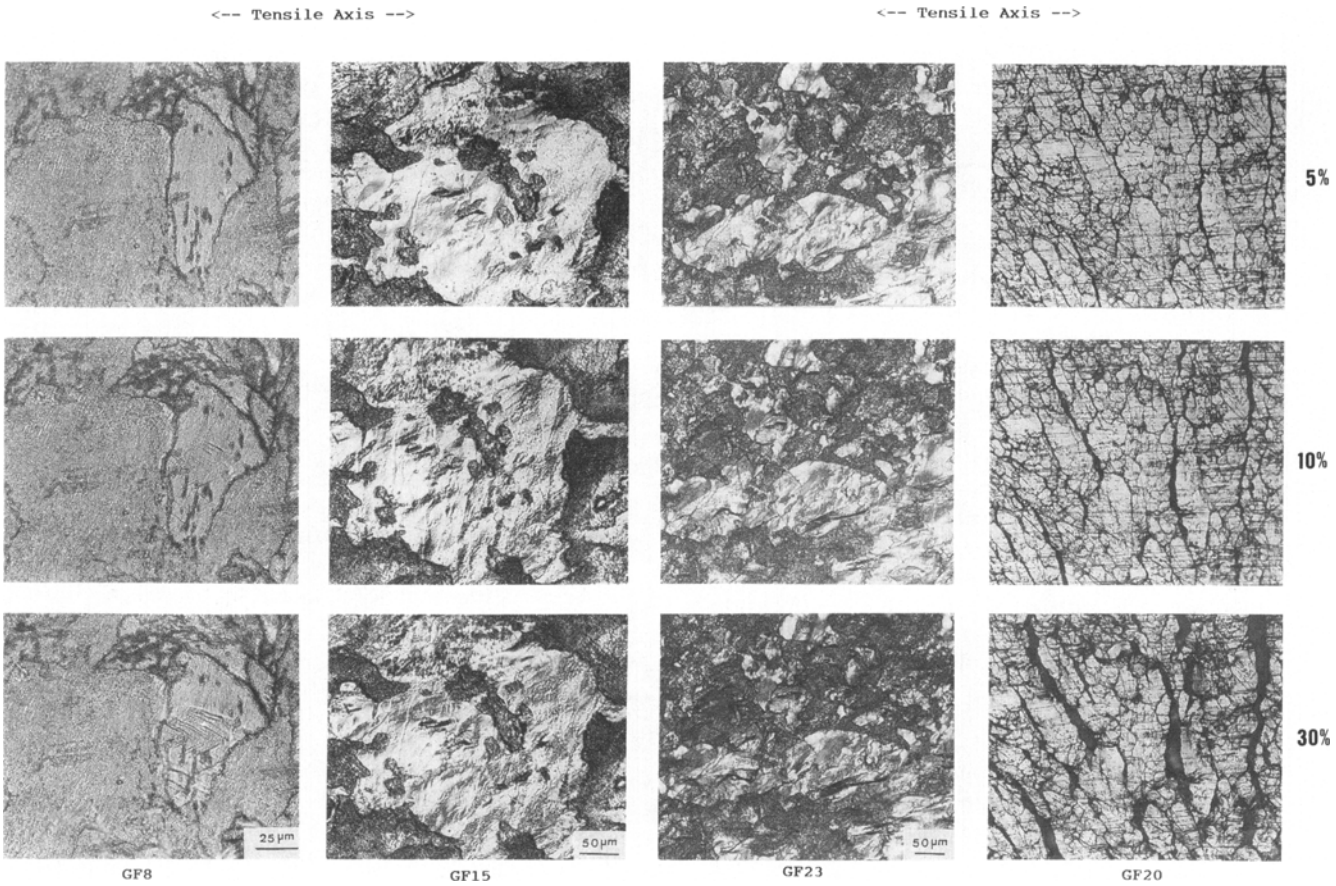

Fig. 4 Optical micrographs of deformed surfaces of Galfan coatings

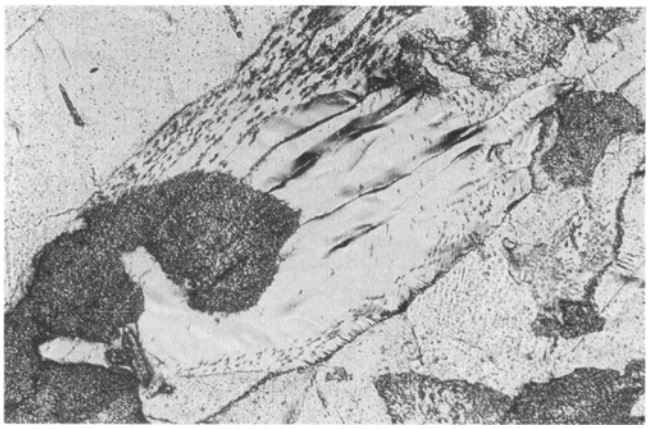

(a)

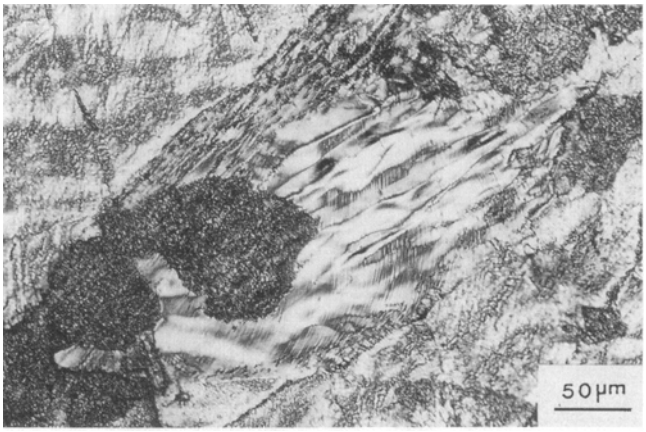

(b)

Fig. 5 Surface of GF15 coating at 15% strain under (a) normal and (b) polarized light

other words, in grains that are more randomly oriented (as in large grain size Galfan coatings), further straining will bring about the formation of cracks in the grain in question. The larger the grain size, the greater is the tendency for the deformation to proceed by a combination of twins and cracks. As a result, less twin-band behavior could be seen in samples with a relatively low basal orientation.

Other reasons for the superior behavior of Galfan coatings during deformation lie in the microstructure. The coatings are almost completely eutectic, and there is no optically detectable intermetallic layer present at the coating-substrate interface. The eutectic cells provide high stored energies to resist transgranular crack propagation and are thus capable of providing uniform deformation under stress.

3.2.3 Galvalume

The results of this study indicate that there are three important sites for crack nucleation in a Galvalume coating: interdendritic zinc-rich regions, spherical shrinkage voids, and silicon flakes. No evidence was found to support the theory of Humayun (Ref 18) that the intermetallic layer assisted crack formation.

(a)

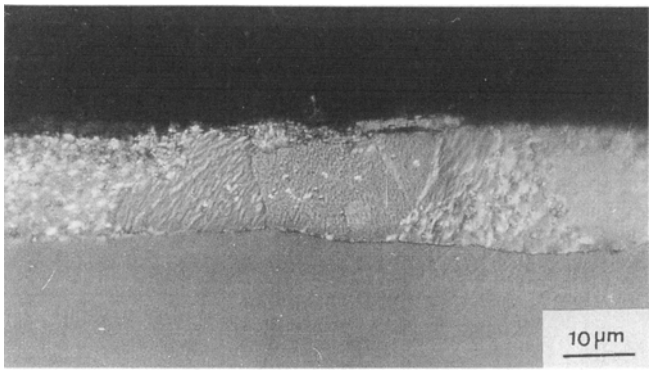

(b)

Fig. 6 Transverse sections of GF15 coating at (a) 5% and (b) 25% strain

The use of SEM confirmed that cracking could be nucleated at low strains in the brittle interdendritic zinc-rich regions (Fig. 8). These cracks grow as plastic strain increases (Fig. 8b). This region, which consists of zinc-rich β-particles within the eutectic structure, is associated with the $(10\bar{1}1)$ orientation. It is therefore possible that some plastic deformation occurred prior to cracking.

Cracks could also be nucleated by shrinkage voids (e.g., Fig. 8a).

Silicon flakes in the coating were also identified as sites for crack nucleation (Fig. 8c), in accordance with a previous observation (Ref 19). However, the severity of this form of cracking can be reduced if the silicon flakes are finely dispersed in the coating during solidification.

A fourth, less significant, mechanism for coating failure is the formation of cracks in large aluminum dendrites at higher strains (Fig. 8b).

3.3 *Coating Plasticity*

Data obtained using the microplasticity method are plotted in Fig. 9, which shows the cracking contribution to total strains as a percentage. Three of the Galfan coatings (8, 15, and 23 μm) show much smaller amounts of cracking than galvanized Galvalume, and the 20 μm thick Galfan material. This can be explained by noting that the less ductile Galfan coating was

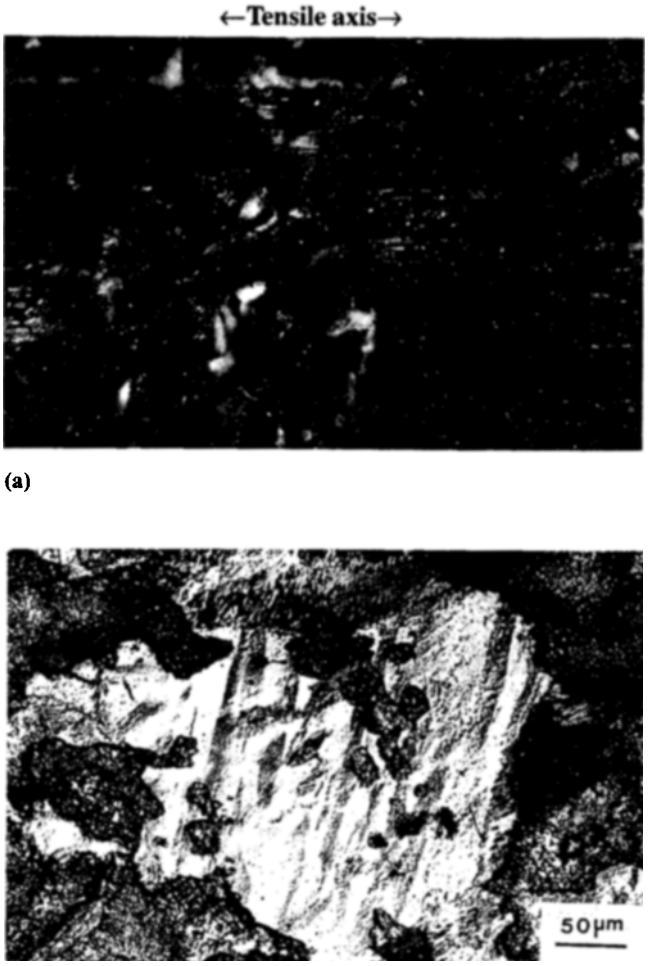

Fig. 7 Twin formation at surfaces of (a) GF20 and(b) GF15 coatings at 5% strain. Optical micrographs using polarized light

produced by a different manufacturer than the other three and contained a different type of microstructure, one with strongly developed grain boundary dents. These would have been prone to initiate separation at grain boundaries when the coating was deformed. The galvanized sample evaluated in this study was a conventional normal spangle product and behaved in a predictable manner, as did the Galvalume product. All coatings showed an increased contribution from the widening of cracks to coating deformation as strain increased. This merely reflects the diminishing ability of the coatings to deform plastically as straining continued.

4. Conclusions

- Hot-dip galvanized coatings deform by slip, twinning, and grain boundary separation at low strains. At higher strains, intragranular cracking becomes important.
- The Galfan samples examined had a strong basal texture that increased with decreased spangle size. The deformation behavior of Galfan coatings depended on the microstructure, texture, and extent of dent formation at the grain boundaries. Initial plastic deformation took place through slip and twinning. Intragranular cracking at higher levels of strain could be associated with the cleavage of basal planes.
- Cracking in the Galvalume coating was found to be initiated at zinc-rich interdendritic regions, spherical voids, and silicon flakes at lower strains, while cracks were also found to form within aluminum dendrites at higher strains.

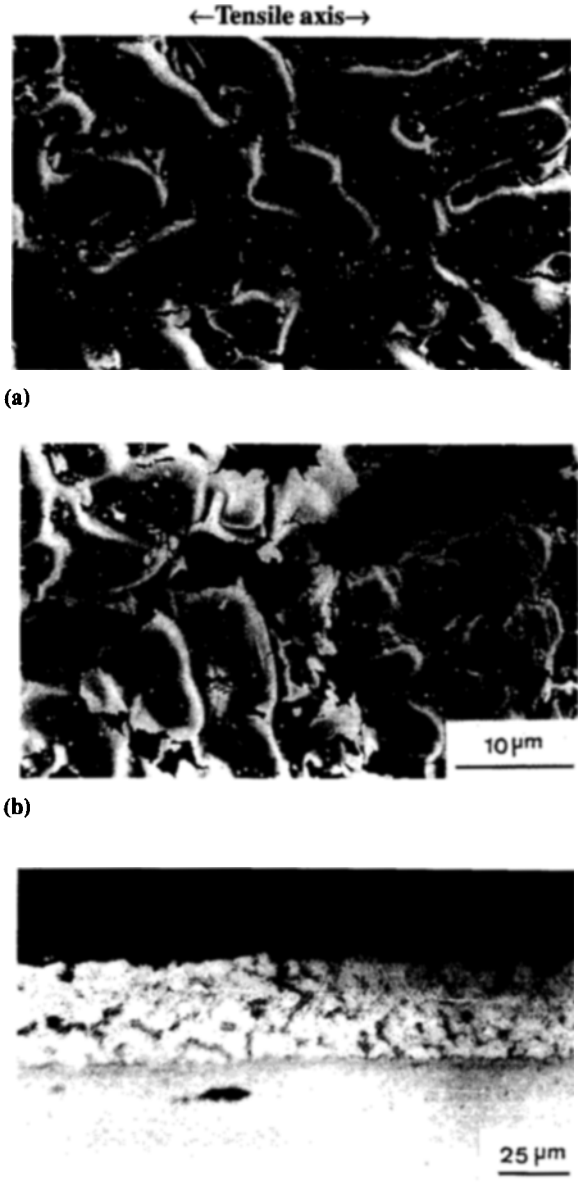

Fig. 8 (a) and (b) Deformed surfaces of Galvalume coating at 10% and 20% strain, respectively. SEM micrographs. (c) Transverse section of Galvalume coating at 10% strain

References

1. P.G. Partridge, The Crystallography and Deformation Modes of Hexagonal Close-Packed Metals, *Mat. Metall. Rev.*, Vol 118, 1967, p 169
2. M.H. Yoo and C.T. Wei, Slip Modes of Hexagonal Close-Packed Metals, *J. Appl. Phys.*, Vol 38, 1967, p 4317

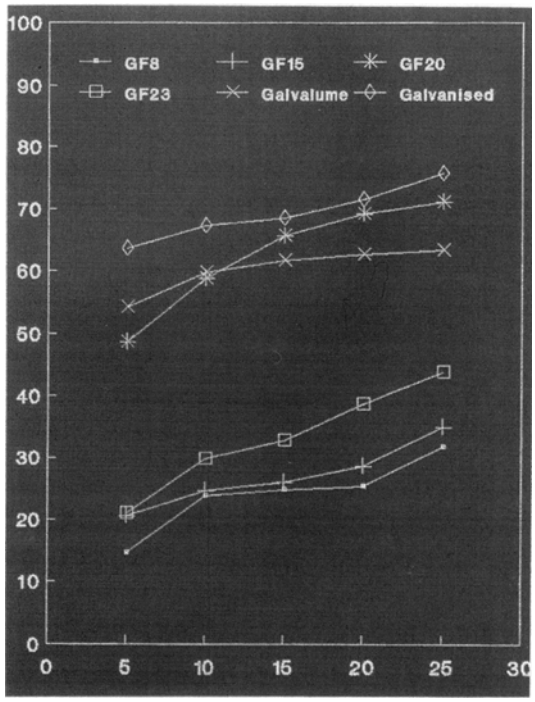

Fig. 9 Coating plasticity of hot-dip zinc and zinc-alloy coatings

3. N. Ecob and B. Ralph, Effect of Grain Size on Flow Stress of Textured Zn-Alloy, *Met. Sci.*, Vol 17, 1983, p 317
4. N.J. Wall, J.A. Spittle, and R.D. Jones, "The Deformation Characteristics of Zinc Coatings on Hot-Dip Galvanized Mild Steel Strip," paper presented at the First Int. Conf. on Zinc-Coated Steel Sheet, Munich, 1985
5. J. Idris, S.R. Shah, J.A. Spittle, and R.D. Jones, "Cracking in Deformed Coated Strip," paper presented at the Second Int. Conf. on Zinc-Coated Steel Sheet, Rome, 1988
6. R.M.S.B. Horta, W.T. Roberts, and D.V. Wilson, Texture Representation by Inverse Pole Figures, *Trans. Metall. Soc. AIME*, Vol 245, 1969, p 2525
7. J. Idris, Ph.D. thesis, University of Wales, 1989
8. D. Jaffrey, J.D. Browne, and T.J. Howard, The Cracking of Zinc Spangles on Hot-Dipped Galvanised Steel, *Metall. Trans.*, Vol 11B, 1980, p 631
9. N.J. Wall, J.A. Spittle, and R.D. Jones, "The Crystallography of the Spangle of Hot-Dipped Galvanised Coatings on Mild Steel Strip," paper presented at the First Int. Conf. on Zinc-Coated Steel Sheet, Munich, 1985
10. D. Jaffrey, J.D. Browne, and L.G. Lock-Lee, "On the Origin of Spangle Cracking," paper presented at the Annual Conf. of the Int. Inst. of Welding, Australia, 1976
11. J. Pelerin, J.P. Servais, D. Coutsouradis, D.C. Herrschaft, and S.F. Radtke, Galfan: A New Zinc-Aluminum Coating, *Proc. 13th Int. Galvan Conf.*, London, ZDA, 1982
12. M. Lamberigts, V. Leroy, M. Kuhn, and L. Renard, "Aluzinc Plus: A New Continuous Hot Dip 55% Al-Zn Protective Coating," paper presented at the Second Int. Conf. on Zinc and Zinc Alloy Coated Steel Sheet (Galvatech '92), Amsterdam, 1992
13. K.L. Lin, J.K. Ho, C.S. Jong, and J.T. Lee, Growth Behavior and Corrosion Resistance of 5% Al-Zn Coating, *Corrosion*, Vol 49 (No. 9), 1993, p 759
14. V. Rangarajan, N.M. Giallourakis, D.K. Matlock, and G. Krauss, The Effect of Texture and Microstructure on Deformation of Zinc Coatings, *J. Mater. Shap. Technol.*, Vol 6, 1989, p 217
15. S.F. Radtke, Galfan—The Total Galvanising Alloy, *Proc. Ann. Meeting Lead Ind. Assoc.*, Missouri, 1982, p 54
16. F.E. Goodwin, A.F. Skenazi, and R.F. Lynch, Corrosion Test Results and Application of Coil Coated Galfan, *CIM Bull.*, Vol 80, 1987, p 115
17. G.J. Harvey, Structure and Corrosion Resistance of Zincalume Coatings, *BHP Tech. Bull.*, Vol 25, 1981, p 63
18. A. Humayun, "Roll-Forming of Metal Coated Sheet Steels," paper presented at the European Coil Coating Association General Assembly, Venice, 1986
19. D.J. Willis, Cracking Characteristics of Zinc and Zinc-Aluminum Alloy Coatings, *Proc. Int. Conf. on Zinc and Zinc-Alloy Coated Steel Sheet (Galvatech '89)*, Tokyo, 1989, p 351